CERN-TH/97-345
JYFL-2/98
hep-ph/9802350

SCALE EVOLUTION OF NUCLEAR PARTON DISTRIBUTIONS

K.J. Eskola[a,b,1], V.J. Kolhinen[a,2] and P.V. Ruuskanen[a,3]

[a] *Department of Physics, University of Jyväskylä, P.O.Box 35, FIN-40351 Jyväskylä, Finland*

[b] *CERN/TH, CH-1211 Geneve 23, Switzerland*

Abstract

Using the NMC and E665 nuclear structure function ratios F_2^A/F_2^D and $F_2^A/F_2^{\rm C}$ from deep inelastic lepton-nucleus collisions, and the E772 Drell–Yan dilepton cross sections from proton-nucleus collisions, and incorporating baryon number and momentum sum rules, we determine nuclear parton distributions at an initial scale Q_0^2. With these distributions, we study QCD scale evolution of nuclear parton densities. The emphasis is on small values of x, especially on scale dependence of nuclear shadowing. As the main result, we show that a consistent picture can be obtained within the leading twist DGLAP evolution, and in particular, that the calculated Q^2 dependence of $F_2^{\rm Sn}/F_2^{\rm C}$ agrees very well with the recent NMC data.

CERN-TH/97-345
JYFL-2/98
February 1998

[1] kjeskola@ux.phys.jyu.fi
[2] kolhinen@ux.phys.jyu.fi
[3] ruuskanen@jyfl.jyu.fi

1 Introduction

Structure function F_2^A has been measured in deep inelastic lepton-nucleus scatterings for a wide range of nuclei A [1]. The ratios of F_2^A to the structure function of deuterium, $F_2^A(x,Q^2)/F_2^D(x,Q^2)$, reveal clear deviations from unity. This indicates that parton distributions of bound nucleons are different from the ones of free nucleons: $xf_{i/A}(x,Q^2) \neq xf_{i/p}(x,Q^2)$. The nuclear effects in the ratio F_2^A/F_2^D are usually divided into the following regions in Bjorken x:

- shadowing; a depletion at $x \lesssim 0.1$,
- anti-shadowing; an excess at $0.1 \lesssim x \lesssim 0.3$,
- EMC effect; a depletion at $0.3 \lesssim x \lesssim 0.7$
- Fermi motion; an excess towards $x \to 1$ and beyond.

At the moment, there is no unique theoretical description of these effects; it is believed that different mechanisms are responsible for them in different kinematic regions. For an overview of the existing data and different models, we refer the reader to Ref. [1].

While the x dependence of the nuclear effects in F_2^A was observed already in the early measurements [2], the Q^2 dependence is much weaker and has therefore been much more difficult to detect. Only recently the first observation of a Q^2 dependence of the ratio $F_2^{\rm Sn}/F_2^{\rm C}$ has been published by the New Muon Collaboration (NMC) [3]. From the point of view of nuclear parton distributions, a high-precision measurement of the scale dependence of F_2^A/F_2^D or $F_2^A/F_2^{\rm C}$ is very important for pinning down the gluon distributions in nuclei [4]. In Ref. [5] preliminary NMC data [6] and the small-x limit of the DGLAP equations [7] were used to determine the gluon ratio $xg_{\rm Sn}/xg_{\rm C}$ from the measured Q^2-evolution of $F_2^{\rm Sn}/F_2^{\rm C}$.

In this paper, our goal is to study whether the observed Q^2 evolution of $F_2^{\rm Sn}/F_2^{\rm C}$ [3] is consistent with the leading twist DGLAP-evolution. By using the data from deeply inelastic lepton-nucleus scattering [8]-[13] and from the Drell–Yan process in pA collisions [14], and by simultaneously requiring baryon number and momentum conservation [4, 15], we will first determine a set of nuclear parton distributions at an initial scale Q_0^2. When doing so, we want to avoid using any specific model for the nuclear effects. We then evolve the initial distributions up to higher scales by using lowest order DGLAP equations without parton fusion corrections [16]. We will show explicitly how the nuclear effects in F_2^A/F_2^D and the similarly defined ratio for the Drell–Yan cross sections evolve in Q^2, and make a comparison with the data. Our procedure leads to a consistent picture, and as the main result, we will show that a very good agreement is obtained between our leading twist QCD approach and the NMC data [3] for the Q^2 dependence of $F_2^{\rm Sn}/F_2^{\rm C}$.

Scale evolution of nuclear effects has been studied already earlier [17, 15, 4] but since then the parton distributions of *proton* have become much better known, especially at small values of x, where a rapid rise of the structure function F_2^p has been observed at HERA [18]. Consequently, also the gluon distributions can be much better determined. So far, there has been no signs in the HERA data for the need of parton fusion corrections [16] to the evolution equations down to $Q^2 \sim 1$ GeV^2 and $x \sim 10^{-4}$ [19]. The situation has also

improved regarding nuclear data; more high-precision nuclear data for several mass numbers A are available [8]-[13] at small values of x where our main interest is focussed. The QCD scale evolution of nuclear effects in parton distributions, especially with specific models for the initial distributions at $Q^2 = Q_0^2$, has been studied in [15, 20, 21]. See also Refs. [22]-[26].

2 Nuclear parton distributions at Q_0^2

As the first task, we determine the nuclear parton distributions at an initial scale Q_0^2 as model-independently as possible. It turns out that some assumptions are needed about the nuclear effects on the initial distributions of individual parton flavours; we will try to be quite explicit on these assumptions.

Fig. 1 illustrates the problem: both the deep inelastic lepton-nucleus data (DIS) and the proton-nucleus Drell–Yan data (DY) lie on some curves in the (x, Q^2)-plane, determined by the kinematical limits and the experimental acceptances. In particular, they are not along a constant Q^2 line, as would be preferable for solving the DGLAP evolution. Therefore, the initial distributions have to be determined iteratively in such a way that the scale evolved distributions are consistent with the data. Like in the case of a free proton, the initial parton distributions at the chosen Q_0^2 serve as nonperturbative input. Our aim here is mainly to see whether a consistent description based on leading twist QCD scale evolution can be obtained. Therefore we do not attempt to implement a χ^2-minimization procedure in determining the initial distributions but plan to return to this in the future.

The ratio of the structure function F_2^A per nucleon in a nucleus A with Z protons and $A - Z$ neutrons, and F_2^D of deuterium can be written as

$$R_{F_2}^A(x,Q^2) \equiv \frac{F_2^A(x,Q^2)}{F_2^D(x,Q^2)} \tag{1}$$

$$= \frac{[F_2^{p/A}(x,Q^2) + F_2^{n/A}(x,Q^2)] + (2Z/A-1)[F_2^{p/A}(x,Q^2) - F_2^{n/A}(x,Q^2)]}{F_2^{p/D}(x,Q^2) + F_2^{n/D}(x,Q^2)}. \tag{2}$$

In the lowest order in QCD-improved parton model $F_2(x,Q^2) = \sum_q e_q^2[xq(x,Q^2) + x\bar{q}(x,Q^2)]$. Below the charm-mass threshold we then have

$$R_{F_2}^A(x,Q^2) = \frac{5(u_A + \bar{u}_A + d_A + \bar{d}_A) + 4s_A + (\frac{2Z}{A} - 1)3(u_A + \bar{u}_A - d_A - \bar{d}_A)}{5(u + \bar{u} + d + \bar{d}) + 4s}, \tag{3}$$

where $u \equiv u(x,Q^2)$ is the known distribution of u quarks in a free proton, and $u_A \equiv u_{p/A}(x,Q^2)$ is the average u-quark distribution in a bound proton of a nucleus A, and similarly for other quark flavours. For isoscalar nuclei $d_{n/A} = u_A$ and $u_{n/A} = d_A$, and in the formula (3) above we have assumed that this is a good approximation for the non-isoscalar nuclei as well. Nuclear (shadowing) effects in deuterium have been neglected in Eq. (3). These have been studied in [28], where it is shown that the shadowing corrections to $(F_2^p + F_2^n)/2$ are of order 1 % at $x \gtrsim 0.007$. Cumulative effects for $x > 1$ will also be neglected as well as the binding energy effects when using $M_A/A \approx m_p \approx m_n$.

We define the nuclear valence quark distributions in a usual way, $q_V^A \equiv q_A - \bar{q}_A$, assuming that any differences between quarks and antiquarks in the nuclear sea [29] can be neglected.

Let us also define the following ratios for each sea- and valence-quark flavour:

$$R^A_{\bar{q}}(x,Q^2) \equiv \frac{\bar{q}_A(x,Q^2)}{\bar{q}(x,Q^2)}, \tag{4}$$

$$R^A_{q_V}(x,Q^2) \equiv \frac{q^A_V(x,Q^2)}{q_V(x,Q^2)}. \tag{5}$$

For later use, it is convenient to define also the corresponding ratios for the total nuclear valence-quark and light sea-quark distributions:

$$R^A_V(x,Q^2) \equiv \frac{u^A_V(x,Q^2)+d^A_V(x,Q^2)}{u_V(x,Q^2)+d_V(x,Q^2)}, \tag{6}$$

$$R^A_S(x,Q^2) \equiv \frac{\bar{u}_A(x,Q^2)+\bar{d}_A(x,Q^2)+\bar{s}_A(x,Q^2)}{\bar{u}(x,Q^2)+\bar{d}(x,Q^2)+\bar{s}(x,Q^2)}, \tag{7}$$

and similarly for the sum $\bar{u}+\bar{d}$, and for the differences (appearing in the non-isoscalar part) $\bar{u}-\bar{d}$ and u_V-d_V

$$R^A_{\bar{u}+\bar{d}}(x,Q^2) \equiv \frac{\bar{u}_A(x,Q^2)+\bar{d}_A(x,Q^2)}{\bar{u}(x,Q^2)+\bar{d}(x,Q^2)}, \tag{8}$$

$$R^A_{\bar{u}-\bar{d}}(x,Q^2) \equiv \frac{\bar{u}_A(x,Q^2)-\bar{d}_A(x,Q^2)}{\bar{u}(x,Q^2)-\bar{d}(x,Q^2)}, \tag{9}$$

$$R^A_{u_V-d_V}(x,Q^2) \equiv \frac{u^A_V(x,Q^2)-d^A_V(x,Q^2)}{u_V(x,Q^2)-d_V(x,Q^2)}. \tag{10}$$

The relations between $R^A_V, R^A_{u_V-d_V}$ and $R^A_{u_V}, R^A_{d_V}$, and between $R^A_{\bar{u}+\bar{d}}, R^A_{\bar{u}-\bar{d}}$ and $R^A_{\bar{u}}, R^A_{\bar{d}}$ are obvious. Then Eq. (3) becomes

$$\begin{aligned} R^A_{F_2}(x,Q^2) &= A^{IS}_V(x,Q^2)R^A_V(x,Q^2) + A^{IS}_{ud}(x,Q^2)R^A_{\bar{u}+\bar{d}}(x,Q^2) + A_s(x,Q^2)R^A_s(x,Q^2) \\ &\quad +(\frac{2Z}{A}-1)[A^{NIS}_V(x,Q^2)R^A_{u_V-d_V}(x,Q^2) + A^{NIS}_{ud}(x,Q^2)R^A_{\bar{u}-\bar{d}}(x,Q^2)], \end{aligned} \tag{11}$$

where the coefficients are known:

$$A^{IS}_V(x,Q^2) = 5[u_V(x,Q^2)+d_V(x,Q^2)]/N_{F_2}(x,Q^2) \tag{12}$$

$$A^{IS}_{ud}(x,Q^2) = 10[\bar{u}(x,Q^2)+\bar{d}(x,Q^2)]/N_{F_2}(x,Q^2) \tag{13}$$

$$A_s(x,Q^2) = 4s(x,Q^2)/N_{F_2}(x,Q^2) \tag{14}$$

$$A^{NIS}_V(x,Q^2) = 3[u_V(x,Q^2)-d_V(x,Q^2)]/N_{F_2}(x,Q^2) \tag{15}$$

$$A^{NIS}_{ud}(x,Q^2) = 6[\bar{u}(x,Q^2)-\bar{d}(x,Q^2)]/N_{F_2}(x,Q^2) \tag{16}$$

$$N_{F_2}(x,Q^2) = 5[u_V(x,Q^2)+d_V(x,Q^2)] + 10[\bar{u}(x,Q^2)+\bar{d}(x,Q^2)] + 4s(x,Q^2). \tag{17}$$

In order to have further constraints for the individual nuclear ratios above, we will consider differential Drell–Yan cross sections in pA collisions. For a nucleus with Z protons and

$A-Z$ neutrons the ratio of cross section to that for deuterium can be written in the lowest order as[4]

$$
\begin{aligned}
R^A_{DY}(x_2,Q^2) &\equiv \frac{\frac{1}{A}d\sigma^{pA}_{DY}/dx_2dQ^2}{\frac{1}{2}d\sigma^{pD}_{DY}/dx_2dQ^2} \\
&= \{4[u_1(\bar{u}^A_2+\bar{d}^A_2)+\bar{u}_1(u^A_2+d^A_2)]+[d_1(\bar{d}^A_2+\bar{u}^A_2)+\bar{d}_1(d^A_2+u^A_2)]+4s_1s^A_2+...\}/N_{DY} \\
&+(\frac{2Z}{A}-1)\{4[u_1(\bar{u}^A_2-\bar{d}^A_2)+\bar{u}_1(u^A_2-d^A_2)]+[d_1(\bar{d}^A_2-\bar{u}^A_2)+\bar{d}_1(d^A_2-u^A_2)]\}/N_{DY} \qquad (18)
\end{aligned}
$$

where

$$
N_{DY}=4[u_1(\bar{u}_2+\bar{d}_2)+\bar{u}_1(u_2+d_2)]+[d_1(\bar{d}_2+\bar{u}_2)+\bar{d}_1(d_2+u_2)]+4s_1s_2+... \qquad (19)
$$

and we have used the notation $q^{(A)}_i \equiv q_{(A)}(x_i,Q^2)$ for $i=1,2$ and $q=u,d,s,....$ The variable Q^2 is the invariant mass of the lepton pair. The target (projectile) momentum fraction is x_2 (x_1), and $x_1=Q^2/(sx_2)$. With the definitions in Eqs. (4)-(10), we obtain

$$
\begin{aligned}
R^A_{DY}(x,Q^2) &= B^{IS}_{ud}(x_1,x_2,Q^2)R^A_{\bar{u}+\bar{d}}(x_2,Q^2)+B^{IS}_V(x_1,x_2,Q^2)R^A_V(x_2,Q^2)+ \\
&+B_s(x_1,x_2,Q^2)R^A_s(x_2,Q^2)+(\frac{2Z}{A}-1)[B^{NIS}_{ud}(x_1,x_2,Q^2)R^A_{\bar{u}-\bar{d}}(x_2,Q^2)+ \\
&+B^{NIS}_V(x_1,x_2,Q^2)R^A_{u_V-d_V}(x_2,Q^2)] \qquad (20)
\end{aligned}
$$

where the coefficients are:

$$
\begin{aligned}
B^{IS}_{ud}(x_1,x_2,Q^2) &= [4(u_1+\bar{u}_1)+d_1+\bar{d}_1](\bar{u}_2+\bar{d}_2)/N_{DY} \qquad (21)\\
B^{IS}_V(x_1,x_2,Q^2) &= (4\bar{u}_1+\bar{d}_1)(u_{V2}+d_{V2})/N_{DY} \qquad (22)\\
B_s(x_1,x_2,Q^2) &= 4s_1s_2/N_{DY} \qquad (23)\\
B^{NIS}_{ud}(x_1,x_2,Q^2) &= [4(u_1+\bar{u}_1)-d_1-\bar{d}_1](\bar{u}_2-\bar{d}_2)/N_{DY} \qquad (24)\\
B^{NIS}_V(x_1,x_2,Q^2) &= (4\bar{u}_1-\bar{d}_1)(u_{V2}-d_{V2})/N_{DY} \qquad (25)\\
N_{DY} &= [4(u_1+\bar{u}_1)+d_1+\bar{d}_1](\bar{u}_2+\bar{d}_2)+4s_1s_2+(4\bar{u}_1+\bar{d}_1)(u_{V2}+d_{V2}) \qquad (26)
\end{aligned}
$$

with $q_{V2}\equiv q_V(x_2,Q^2)$ and $q_1=q_V(x_1,Q^2)+\bar{q}(x_1,Q^2)$, $q=u,d$.

The DIS data [8, 10, 11, 3] which we use in determining the nuclear ratios, are approximately corrected for non-isoscalar effects, so we may consider isoscalar nuclei first. In Eqs. (11) and (20) the terms proportional to $(2Z/A-1)$ can be dropped, and we are left with $R^A_V, R^A_{\bar{u}+\bar{d}}$ and R^A_s only. Without additional information we cannot fix three ratios from two equations. Further constraints could in principle be obtained from the measurements of nuclear structure functions $F^{\nu A}_2/F^{\nu D}_2$ and $F^{\nu A}_3/F^{\nu D}_3$ with neutrino beams [30], but more statistics and mass number systematics would be needed. Instead, as a first approximation, we take for the sea quarks $R^A_s(x,Q^2_0)=R^A_{\bar{u}+\bar{d}}(x,Q^2_0)$. For evolving each flavour separately, we will also assume that initially $R^A_{\bar{q}}(x,Q^2_0)=R^A_S(x,Q^2_0)$, and similarly for the valence quarks $R^A_{u_V}(x,Q^2_0)=R^A_{d_V}(x,Q^2_0)=R^A_V(x,Q^2_0)$. It should be emphasized that this approximation is

[4]In Ref. [4], the corresponding formula is incorrect, but it has the correct large-x_F limit, which was used only.

needed *only* at the initial scale Q_0^2, in determining the initial distributions for the DGLAP evolution. In this paper we use, for simplicity, the parton distribution set GRV-LO [31], where the massive quarks evolve as massless ones above each mass-threshold. This set also assumes $\bar{u} = \bar{d}$, so $R_{\bar{u}}^A = R_{\bar{d}}^A$ at all scales for this particular set.

In this approximation, we obtain two equations for the ratios at an initial scale Q_0^2,

$$R_{F_2}^A(x,Q_0^2) = A_V^{IS}(x,Q_0^2)R_V^A(x,Q_0^2) + [A_{ud}^{IS}(x,Q_0^2) + A_s(x,Q_0^2)]R_S^A(x,Q_0^2), \quad (27)$$

$$R_{DY}^A(x,Q_0^2) = B_V^{IS}(x_1,x,Q_0^2)R_V^A(x,Q_0^2) + [B_{ud}^{IS}(x_1,x,Q_0^2) + B_s(x_1,x,Q_0^2)]R_S^A(x,Q_0^2) \quad (28)$$

where Q_0^2 is chosen below the charm threshold. Eqs. (27) and (28) would fix R_V^A and R_S^A if the DIS and DY data would lie at the same values of x and Q_0^2. Since this is not the case (see Fig. 1), the initial profiles $R_S^A(x,Q_0^2)$ and $R_V^A(x,Q_0^2)$ are determined iteratively after comparing the evolved distributions with the data. As is clear from Eqs. (27) and (28), the initial nuclear ratios acquire some dependence on the particular parton distribution set used for the proton. With the modern sets, however, this dependence can be expected to be quite weak.

As a further constraint for nuclear valence quarks [15, 4], baryon number conservation

$$\int_0^1 dx[u_V(x,Q_0^2) + d_V(x,Q_0^2)]R_V^A(x,Q_0^2) = \int_0^1 dx[u_V(x,Q_0^2) + d_V(x,Q_0^2)] = 3. \quad (29)$$

will also be required [15, 4].

In practice, our iteration procedure for determining the ratios $R_S^A(x,Q_0^2)$ and $R_V^A(x,Q_0^2)$ proceeds with the following steps:

- make an ansatz for $R_{F_2}^A(x,Q_0^2)$ based on the DIS data;
- decompose $R_{F_2}^A(x,Q_0^2)$ into R_V^A and R_S^A, and constrain R_V^A with baryon number conservation;
- estimate $R_G^A(x,Q_0^2)$ (see the discussion below);
- perform DGLAP evolution with the obtained initial nuclear parton distributions;
- constrain $R_S^A(x,Q_0^2)$ and $R_V^A(x,Q_0^2)$ with the DY data.

First, we introduce an initial parametrization for $R_{F_2}^A(x,Q_0^2)$. We choose $Q_0^2 = 2.25$ GeV^2, which is the charm-mass threshold for the GRV-LO set. Rather than trying to make a separate analysis for each nucleus, we parameterize also the A dependence of $R_{F_2}^A$. The functional form is given in the Appendix. Note also, that as the existing parametrizations [32, 33] are fits to the data along the kinematical curves in Fig. 1, we cannot use them directly for obtaining the distributions at fixed scale Q_0. Furthermore, we have to make an assumption on the behaviour of $R_{F_2}^A(x,Q_0^2)$ at $x \lesssim 10^{-3}$. In this region a saturation of shadowing has been observed [12, 9] at nonperturbative scales, $\langle Q^2 \rangle \ll Q_0^2$ (see Figs. 1 and 5). Motivated by this, we will also assume saturation of shadowing in $R_{F_2}^A(x,Q_0^2)$, keeping in mind, however, that consistency of this assumption must be verified after evolving the distributions (see Figs. 4).

We then decompose $R^A_{F_2}$ into R^A_V and R^A_S according to Eq. (27). First observation is that we cannot have $R^A_V = R^A_{F_2}$ at all values of x, because up to 9 % of baryon number would be missing for the heaviest nuclei. Second observation is that $R^A_{F_2} \approx R^A_V\,(R^A_S)$ at large (small) values of x. In practice, in the region of large (small) x, it becomes impossible to determine $R^A_S\,(R^A_V)$ directly from the data for $R^A_{F_2}$, because of the negligible sea (valence)-quark contribution. Therefore, we apply a piecewize construction: at $x < x_p \sim 0.1$ we fix R^A_V with the same functional form as for $R^A_{F_2}$ but with different parameters. Then, through Eq. (27) R^A_S becomes fixed. At $x_p < x < x_{eq} \sim 0.4$ we fix R^A_S in turn, with a simple form of a plateau $R^A_S(x_p < x < x_{eq}, Q^2_0) = R^A_S(x_p, Q^2_0)$. Now the approximate plateau in R^A_S controls the height of the anti-shadowing peak in R^A_V. At $x = x_{eq}$ the sea-quark ratio $R^A_S(x_p, Q^2_0)$ becomes equal to $R^A_{F_2}(x_p, Q_0)$, and at $x > x_{eq}$, in lack of further information on R^A_S, we again use the simplest approximation $R^A_V = R^A_S = R^A_{F_2}$. The precise values of x_p and x_{eq}, (i.e. the location and height of the plateau in R^A_S), together with the parameters for R^A_V are first constrained by the baryon number conservation at $Q^2 = Q^2_0$ and after the DGLAP evolution by the DY data [14].

Finally, we define the nuclear gluon ratio by

$$R^A_G(x, Q^2) \equiv g_A(x, Q^2)/g(x, Q^2), \tag{30}$$

and specify $R^A_G(x, Q^2_0)$ to have the full input for the DGLAP evolution. We constrain $R^A_G(x, Q^2_0)$ with momentum conservation [15, 4]:

$$1 = \int_0^1 dx\, x\Big\{g(x, Q^2_0)R^A_G(x, Q^2_0) + [u_V(x, Q^2_0) + d_V(x, Q^2_0)]R^A_V(x, Q^2_0) + 2[\bar{u}(x, Q^2_0) + \bar{d}(x, Q^2_0) + s(x, Q^2_0)]R^A_S(x, Q^2)\Big\}, \tag{31}$$

where R^A_V and R^A_S are determined as described above. Compared to free nucleons, we find that some momentum is transferred from quarks to gluons in nuclei. This effect is not very large: in $A = 208$ the glue carries about 4 % more momentum than in a free nucleon. This is in agreement with the earlier studies [15, 4]. Consequently, without any x-dependence in $R^A_G(x, Q^2_0)$ we would have $R^A_G(x, Q^2_0) = 1.04$.

Since the sea quarks are shadowed at small x, we expect shadowing of the nuclear gluons as well. A requirement of stable scale evolution can be used together with the recent NMC data [3] to further constrain nuclear gluon shadowing. At the small-x limit of the DGLAP equations one obtains

$$\frac{\partial R^A_{F_2}(x, Q^2)}{\partial \log Q^2} = \frac{\partial F^D_2(x, Q^2)/\partial \log Q^2}{F^D_2(x, Q^2)}\Big\{\frac{\partial F^A_2(x, Q^2)/\partial \log Q^2}{\partial F^D_2(x, Q^2)/\partial \log Q^2} - R^A_{F_2}(x, Q^2)\Big\} \tag{32}$$

$$\approx \frac{5\alpha_s}{9\pi}\frac{xg(2x, Q^2)}{F^D_2(x, Q^2)}\Big\{R^A_G(2x, Q^2) - R^A_{F_2}(x, Q^2)\Big\}, \tag{33}$$

where we have used the result $\partial F_2(x, Q^2)/\partial \log Q^2 \approx 5\alpha_s xg(2x, Q^2)/9\pi$, derived in [34]. As for the initial $R^A_{F_2}(x, Q^2_0)$, we will also assume a saturation in shadowing of the glue, so that $R^A_G(2x, Q^2_0) \approx R^A_G(x, Q^2_0)$ at the limit $x \to 0$. For the GRV-LO set we are using, the ratio $xg(2x, Q^2_0)/F_2(x, Q^2_0)$ is non-zero and grows slowly at small values of x, so $R^A_{F_2}$ evolves

towards R_G^A due to the factor $R_G^A - R_{F_2}^A$ in Eq. (33). An initial condition stable in the evolution is obtained by requiring $R_G^A(x,Q_0^2) \approx R_{F_2}^A(x,Q_0^2)$ at very small values of x.

Due to momentum conservation, the loss of gluons in the shadowing region must lead to an increase of gluon distribution somewhere at larger x. In Ref. [4], it was assumed that $R_G^A(x,Q^2)$ is constant at large x. This, however, resulted in somewhat unstable profiles for R_G^A and R_S^A in the evolution. Therefore, we expect that there is an EMC-effect also for the glue, and that $R_G^A(x,Q_0^2)$ is peaked around the same values as $R_V^A(x,Q_0^2)$ and $R_S^A(x,Q_0^2)$.

In practice, we determine the gluon ratio as follows. We start with $R_G^A(x,Q_0^2) \approx R_{F_2}^A(x,Q_0^2)$ at small values of x. Should we use this equality for all values of x, some momentum would be missing for all nuclei (11 % for $A=208$). This indicates that conservation of momentum requires quite strong anti-shadowing for the gluons. For $R_G^A(x,Q_0^2)$ we use the functional form given in the Appendix. In determination of the position and width of the anti-shadowing peak (which we assume to be independent of A) we use Ref. [5] to constrain the value of x where $xg_{\rm Sn}/xg_{\rm C} \approx 1$. The amount of anti-shadowing then follows from momentum conservation, leading to a good agreement with Ref. [5] once the position and width parameters of the peak in R_G^A are fixed.

The initial nuclear ratios $R_G^A(x,Q_0^2), R_V^A(x,Q_0^2)$ and $R_S^A(x,Q_0^2)$ at $Q_0^2 = 2.25$ GeV^2 are shown for isoscalar nuclei in Fig. 2 together with the ratios $R_{F_2}^A(x,Q_0^2)$. Correlations in these ratios are easily understood from the figures: the more R_V^A is shadowed, the more it has anti-shadowing, and the more R_S^A is suppressed in the anti-shadowing region. Similarly, due to momentum conservation, the more shadowing R_G^A has, the more anti-shadowing is needed. As seen in the figures, there is more anti-shadowing and less shadowing for R_V^A than for $R_{F_2}^A$. Correspondingly, R_S^A is more shadowed and not anti-shadowed at all at $Q_0^2 = 2.25$ GeV^2. The gluon ratios R_G^A turn out to be clearly more anti-shadowed than $R_{F_2}^A$ and R_V^A. In comparison with the earlier studies, the lack of sea-quark anti-shadowing agrees with [15, 4]. We get, however, somewhat more anti-shadowing for gluons than in [15, 4], which is a consequence of the small-x enhancement of gluon densities in a proton.

3 Scale evolution and results

Scale evolution is straightforward to carry out once the parton fusion corrections [16] are neglected. In the HERA data for $F_2^p(x,Q^2)$ [18, 19] there is no evidence of the fusion corrections at $Q^2 \gtrsim 1$ GeV^2 and $x \gtrsim 10^{-4}$. For nuclei, parton fusion should be stronger due to its expected $A^{1/3}$ scaling [16, 25], but since we start the evolution at $Q_0^2 = 2.25$ GeV^2 > 1 GeV^2, the effects of these corrections should be small [4], at least in the x range of the NMC data [3]. The role of the fusion corrections is, however, a very interesting question [17, 4, 20, 25] which deserves further analyses with constraints for the proton from the new HERA data [35] at very small Q^2 and very small x.

We use the parametrization of GRV-LO [31] for the initial parton distributions of free protons. We evolve these and the initial nuclear distributions from $Q_0^2 = 2.25$ GeV^2 to $Q^2 \sim 10000$ GeV^2 by using the DGLAP equations for gluons and valence and sea quarks of each flavor. Massive quarks are generated through the evolution above each mass threshold as in [31]. We solve the evolution equations directly in (x,Q^2)-space. The resulting scale evolution of the ratios R_G^A, R_S^A and R_V^A is shown in Figs. 3 for $A=208$. Compared with an

earlier study [4], the difference in the evolution of R_G^A and $R_{F_2}^A$ is not as dramatic, due to the enhanced, more stable gluon and sea-quark distributions at small vales of x.

In Figs. 4 we plot the scale evolution of the ratio $R_{F_2}^A(x,Q^2)$ for isoscalars ${}^4_2$He, ${}^{12}_6$C, ${}^{40}_{20}$Ca and for an artificial isoscalar nucleus $A=208$ at different fixed Q^2. The data shown and used in the analysis, are the re-analyzed data from NMC [8] and SLAC [11]. For a more transparent comparison, we show our calculation with filled circles at Q^2 equal to the $\langle Q^2\rangle$ of the NMC data at different x.

In Fig. 5, we show the behaviour of $R_{F_2}^A(x,Q^2)$ at very small x, together with the NMC data [9] and [8] for ^{12}C. This figure confirms the consistency of our initial assumption of the saturation of shadowing in $R_{F_2}^A(x,Q_0^2)$: at fixed x, shadowing decreases with increasing Q^2 and therefore our initial $R_{F_2}^A(x,Q_0^2)$ should not lie below the data measured at $Q^2 < Q_0^2$. This of course implies an implicit assumption that the scale dependence of $R_{F_2}^A$ in the nonperturbative region is towards the same direction as in the perturbative region. It should be kept in mind, however, that at $Q^2 > Q_0^2$ the sign of $\partial R_{F_2}^A(x,Q^2)/\partial Q^2$, as indicated by Eq. (33), actually depends on the gluon shadowing at small x, i.e. if the gluons were more shadowed, the decrease of shadowing in $R_{F_2}^A$ would be slower, or shadowing could even increase. In this case $R_{F_2}^A(x,Q_0^2)$ should be re-determined accordingly. In this way, as pointed out in [4], at small values of x the scale evolution of $R_{F_2}^A$ reflects the amount of nuclear gluon shadowing.

Small-x data for $R_{F_2}^A$ exist also from the E665 collaboration [13], but they lie above the NMC data (see e.g. [10]). Because of the smaller error bars in the NMC data, we decided not to use the absolute E665 data for determining $R_{F_2}^A(x,Q_0^2)$ here. However, as pointed out in [10], if one considers the *ratios* of different nuclei, the two data sets are consistent. Therefore, we have also used the ratio $F_2^{\rm Pb}/F_2^{\rm C}$ as obtained from the E665 data [13]. In Fig. 6 we show the results at small x as in Fig. 5 but for the ratio of ratios, $R_{F_2}^{\rm Pb}/R_{F_2}^{\rm C}$ with the data from [10] and [13]. Note that the inner (outer) error bars under(over)estimate the real errors of the E665 data (see the figure caption). Even without a more precise χ^2 minimization, this figure partly helps us in constraining the A dependence at small values of x in the parametrization of $R_{F_2}^A$ given in the Appendix.

The systematics in nuclear mass number A, especially at $x \lesssim 0.1$, is presented by the NMC collaboration in [10], and we have also made use of these data. In Figs. 7 we show the scale evolution of $F_2^A/F_2^{\rm C}$, i.e. of $R_{F_2}^A/R_{F_2}^{\rm C}$, and the comparison with the NMC data. Since the data are (approximatively) corrected for non-isoscalar effects, we have always $A=2Z$. In our analysis, the data for the $(A=117)$/C ratio gives the most stringent constraints. Again, for an easier comparison, the filled symbols show our calculation at the $\langle Q^2\rangle$ of the data at different x.

How the Drell–Yan data from the E772-collaboration [14] enters our analysis, can be seen from Figs. 8 where we have plotted the ratio of Drell–Yan cross sections as defined in Eq. (20) at different invariant masses Q^2 for ${}^{12}_6$C, ${}^{40}_{20}$Ca, ${}^{56}_{26}$Fe and ${}^{184}_{74}$W. The non-isoscalar terms for Fe and W have been taken into account according to Eq. (20), by using the corrections obtained with isoscalar nuclei. As before, the filled symbols show our calculation at the mass values $\langle Q^2\rangle$ of the data [27]. The constraint for determining the initial ratios $R_S^A(x,Q_0^2)$ and $R_V^A(x,Q_0^2)$ enters as follows: let us suppose that valence quarks are shadowed less than in Figs. 2. This leads to a smaller anti-shadowing for $R_V^A(x,Q_0^2)$ because of baryon number

conservation, Eq. (29). At the same time, Eq. (3) brings $R_S^A(x,Q_0^2)$ closer to $R_{F_2}^A$ at $x\sim 0.1$, i.e. R_S^A becomes less suppressed. In the scale evolution, there is a cross-over region in R_{DY}^A where evolution is very weak (see Figs. 8), and the location of which depends on the plateau in $R_S^A(x\sim 0.1,Q_0^2)$. With less suppressed R_S^A at $x\sim 0.1$, the location of the cross-over region shifts to larger x. Consequently, the evolution of R_{DY}^A becomes too fast at small values of x, and the calculated values overshoot the data. On the other hand, if R_V^A is much more shadowed than in Figs. 2, the cross-over region in R_{DY}^A shifts to the left, scale evolution becomes too fast at $x\gtrsim 0.1$, and the calculation falls below the data. Iterating between these possibilities we have obtained the initial $R_S^A(x,Q_0^2)$ shown in the figures.

In Fig. 9, comparison with the results of Ref. [5] for the gluon ratio $g_{\rm Sn}/g_{\rm C}$ is shown. Again, the curves are plotted at fixed values of Q^2 and the filled symbols show our calculation at the $\langle Q^2\rangle$ of the preliminary NMC data [6] as quoted in [5]. It should be noted that even though only the point where $g_{\rm Sn}/g_{\rm C}\sim 1$ was constrained to agree with [5], the resulting amount of shadowing and anti-shadowing comes out in a very good agreement with the results of Gousset and Pirner.

Finally, in Figs. 10, we present the main result of our study, comparison of the calculated scale evolution of $F_2^{\rm Sn}/F_2^{\rm C}$ with the recent NMC data [3]. The data is plotted with statistical errors only because we are more interested in the slopes of Q^2 evolution than in the absolute normalization to the data. Notice that normalization of our curves at each fixed x in Figs. 10 depends on the initial ratio shown for Sn/C in Fig. 7. In fact we obtain a fairly good agreement also for the overall normalization of the data. The changes in the sign of $\partial(F_2^{\rm Sn}/F_2^{\rm C})/\partial Q^2$ do not seem to be in contradiction with the data, either. It is also interesting to notice that at small values of x the slope is not linear in $\log Q^2$.

After performing the scale evolution, let us look back into the assumptions made in constraining the nuclear ratios at the initial scale Q_0^2. As expected on the basis of Eq. (33), the approximation $R_G^A=R_{F_2}^A$ for the initial distributions at extremely small x turns out to be quite stable in the evolution; at the smallest x we consider, $x=10^{-6}$, deviations from $R_G^A=R_{F_2}^A$ are only about 5 % up to $Q^2=10000$ GeV^2 for $A=208$. For the valence quarks, the initial approximations $R_{u_V}^A=R_V^A(x,Q_0^2)$ and $R_{d_V}^A=R_V^A(x,Q_0^2)$ are very stable: deviations are within 1 % at $x<0.7$ at all scales considered. For the GRV-LO set [31], there is no difference between $\bar{u}$ and $\bar{d}$, so once the initial approximation $R_{\bar{u}}^A=R_{\bar{d}}^A$ is made, it holds exactly at all scales. The initial approximation $R_{\bar{u}+\bar{d}}^A=R_S^A$ is also a stable one, the deviations are within 2 % during the evolution. Initial approximation $R_{\bar{s}}^A=R_S^A$ is slightly less stable, but deviations do stay within 7 % at all scales considered. The deviations are concentrated in the region $x=0.01...0.1$, where the nuclear effects for sea quarks are small in any case. During the evolution, the strange quarks tend to develop more anti-shadowing than R_S^A, while the $\bar{u}$ and $\bar{d}$ have an opposite tendency relative to R_S^A. More work is needed to relax the assumption $R_s^A(x,Q_0^2)=R_{\bar{u}+\bar{d}}^A(x,Q_0^2)$ but this additional correction is beyond the scope of this study.

4 Discussion and Conclusions

The main emphasis of this study is in the Q^2-evolution of nuclear effects in parton distributions in the region of small x. We have used the deep inelastic scattering data from lA

collisions [8]-[13] and the Drell–Yan dilepton data from pA collisions [14] together with conservation of baryon number and momentum to constrain the initial nuclear distributions as model-independently as possible. As the main result, we have shown that a consistent picture arises, and a very good — almost surprisingly good — agreement with the measured Q^2 evolution of the structure function ratio $F_2^{\rm Sn}/F_2^{\rm C}$ [3] can be obtained already with the lowest order leading twist DGLAP evolution. We can therefore conclude that the effect of parton fusion corrections in the evolution [16] is negligible, at least at $x \gtrsim 0.01$ and $Q^2 > 2.25$ GeV^2. In this region, the nuclear modifications are effectively built in the nonperturbative initial conditions for the DGLAP evolution. This result also agrees with Ref. [20].

We point out, however, that even though we obtain a very good agreement with the NMC data [3] and with the analysis of Ref. [5], we can confirm our initial assumption of gluon shadowing at small values of x only on fairly qualitative grounds (stability of the evolution), rather than through a direct comparison with the data. The reason for this is seen qualitatively from Eq. (33): the data on $F_2^{\rm Sn}/F_2^{\rm C}$ at $x = 0.0125$ constrains R_G^A at $x = 0.025$, which is only the beginning of the gluon shadowing region and where nuclear effects in R_G^A are not very strong (see Figs. 2). To constrain the gluon shadowing further, it would be very important to have data for the Q^2 dependence of $F_2^{\rm Sn}/F_2^{\rm C}$ available at smaller values of x.

The NMC data on deep inelastic J/Ψ-production in Sn/C [36] is not included in our analysis but it is interesting to notice, as pointed out in [5], that the amount of gluon anti-shadowing in the ratio Sn/C agrees with the excess reported in [36]. The gluon anti-shadowing we obtain is also consistent with the E789 data on D meson production in pA collisions [37], although the error bar on the data point is quite large. With the strongly interacting final states, higher twist production mechanisms [38] may well make the picture more complicated regarding factorization. However, if the initial state effects can be factorized into the nuclear parton densities [39], our analysis on R_G^A should be of direct use also for computing strongly interacting final states in nuclear collisions. Our results should also provide more insight in understanding the recently measured increase in J/Ψ suppression relative to the Drell–Yan background in central Pb-Pb collisions at the CERN SPS [40].

Nuclear structure functions $F_2^{\nu Fe}$, $F_3^{\nu Fe}$ [41] are used in the global analyses of parton distributions for a *free* proton [42]. Our results should offer a more consistent way of unfolding the nuclear effects there.[5] Also the coordinate space description of nuclear parton densities [43] could be studied in more detail by using the scale evolved nuclear ratios we have presented here. Related to the coordinate space description and scale evolution of nuclear parton distributions, the connection of our results with those in the region of very small x and very large A where the higher twist terms can be expected to be more important [26], should also be studied in more detail.

To conclude, the results of our study are encouraging. They show that further QCD-analysis on nuclear parton distributions is worth performing. For a more detailed analysis, this study can be improved in obvious ways: A more quantitative error analysis should be done by performing a minimization of χ^2 in fits to the data. In determining the nuclear gluon distributions by using the NMC data [3] in a more consistent manner such analysis would be required. Also more work remains to be done in determining the nuclear ratios

[5] We thank C.A. Salgado for discussions on this point.

for individual quark flavors. This should be done, however, model-independently by using the measured data wherever possible. More systematics on mass number dependence of the structure functions $F_2^{\nu A}$ and $F_3^{\nu A}$ and increased statistics against deuterium would be helpful in extracting the nuclear ratios of individual parton distributions (see also [44]). Also data on F_2^A/F_2^D (or e.g. $F_2^A/F_2^{\rm C}$), not corrected for non-isoscalar effects, might be useful for constraining the difference between R_u^A and R_d^A, provided that precision of the data is sufficient. Naturally, further measurements of the Drell–Yan cross sections in pA collisions with more statistics would be very useful.

We do not expect the nuclear ratios to depend strongly on the choice for the (modern) parton distributions of the *free* proton, but an explicit study of this is in progress. For numerical applications we are also preparing a package which produces scale dependent nuclear ratios $R_f^A(x,Q^2)$ for any parton flavour f in an arbitrary nucleus A [45].

Eventually, our analysis should be extended to next-to-leading order in the cross sections and in the scale evolution[6]. It will also be interesting to study the role of the parton fusion corrections in more detail in the light of the HERA results.

Acknowledgements. We thank W. Krasny, C. Lourenço, C.A. Salgado, G. Schuler, G. Smirnov, M. Strikman, R. Venugopalan and M. Vänttinen for useful discussions, and P. McGaughey for providing us with the $\langle Q^2\rangle$-values of the E772 Drell–Yan data. We are grateful to the CFIF and GTAE centers of the Technical University of Lisbon for hospitality during the Hard Probe meeting in September 1997, where part of this work was discussed and developed. We also thank the members of the Hard Probe Collaboration for helpful discussions, comments and encouragement. This work was supported by the Academy of Finland, grant no. 27574.

Appendix

We use the following piecewize parametrization for the ratio $R_{F_2}^A(x,Q_0^2)$, motivated by [4, 33]:

$$R_{F_2}(x,A) = 1 + s(x,A) + \mathrm{emc}(x,A) + f(x,A), \tag{34}$$

with the shadowing part given by

$$s(x,A) = [s_0(x,A) - 1]\mathrm{e}^{-x^2/x_0^2}\Theta(x_m - x), \tag{35}$$

where Θ is a step function, and

$$s_0(x,A) = \frac{1 + a_s k_2(1/x - 1/x_{se})p(x)}{1 + a_s A^{p_2}(1/x - 1/x_{se})p(x)}, \tag{36}$$

and $p(x) = \max[1, (x/x_{se})^{p_3}]$ and $p_3 \geq 0$.

The emc-part is controlled by a function

$$\mathrm{emc}(x,A) = (a_0 + a_1 x + a_2 x^2 + a_3 x^3 - 1)(1 - \mathrm{e}^{-(x/x_{0e}^A)^2})\Theta(x_m - x), \tag{37}$$

[6]NLO evolution of nuclear parton distributions is studied in [20]

parameter	$R^A_{F_2}(x,Q_0^2)$	$R^A_V(x<x_p,Q_0^2)$
x_{se}	0.075	0.028
x_0	0.10	0.11
$x^{\rm C}_{0e}$	0.14	0.14
x_e	0.32	0.32
x_m	0.74	0.74
x_f	0.84	0.84
a_s	0.016	0.019
k_2	1.1	1.03
p_2	0.113	0.03
p_3	0.3	0.3
p_e	0.05	0.05
$f^{\rm Ca}_m$	0.87	0.87

Table 1: The parameters used for $R^A_{F_2}(x,Q_0^2)$ and $R^A_V(x<x_p,Q_0^2)$ with $x_p=0.09$ (see Sec. 2).

where $x^A_{0e}=x^{\rm C}_{0e}(A/12)^{p_e}$. We fix the location of the minimum in $R_{F_2}(x,A)$ at $x_m=0.74$ for all nuclei. With the parameter x_0 for $s(x,A)$ and with the parameter x^A_{0e} for emc(x,A), we obtain a smoothly behaving anti-shadowing region in $R_{F_2}(x,A)$.

The Fermi-motion region is parametrized with

$$f(x,A)=\Big[(1-f^A_m)\frac{(x-x_m)^2}{(x_f-x_m)^2}+f^A_m-1\Big]\Theta(x-x_m) \tag{38}$$

with $f^A_m=f^{\rm Ca}_m(A/40)^\alpha$, where α is given by Eq. (9) of Ref. [11] with $x=x_m$. For simplicity, we have fixed $R_{F_2}(x_f,A)=1$ for all nuclei.

The parameters a_0,a_1,a_2,a_3 above are determined from the following conditions:

$$e(x_e)=1,\quad e(x_m)=f^A_m,\quad \frac{\partial e(x)}{\partial x}\Big|_{x=x_{0e}}=0,\quad \frac{\partial e(x)}{\partial x}\Big|_{x=x_m}=0, \tag{39}$$

where $e(x)=a_0+a_1x+a_2x^2+a_3x^3$. In the Table 1 below, we give the parameters for the parametrizations of $R^A_{F_2}(x,Q_0^2)$ and $R^A_V(x<x_p,Q_0^2)$.

The form of the initial nuclear gluon ratio $R^A_G(x,Q_0^2)$ is the following:

$$\begin{aligned} R^A_G(x,Q_0^2) &= R_{F_2}(x,A)\Big\{1+N\Big[\exp\Big(-\frac{(\log x-(\log x_g-\Delta_g/1.5))^2}{\Delta_g^2}\Big)+ \\ &\qquad \exp\Big(-\frac{(\log x-(\log x_g+\Delta_g/1.5))^2}{\Delta_g^2}\Big)\Big]\Big\}, \end{aligned} \tag{40}$$

where x_g gives the position for the additional anti-shadowing bump in R^A_G, and Δ_g determines its width in $\log x$. The amplitude N for the enhancement can be directly determined by using the momentum sum rule (31). In Figs. 2, we have $x_g=0.09$ and $\Delta_g=0.9$.

References

[1] M. Arneodo, Phys. Rep. **240** (1994) 301.

[2] EMC collaboration, J.J. Aubert *et al.*, Phys. Lett. **B123** (1983) 275; A. Bodek *et al.*, Phys. Rev. Lett. **50** (1983) 1431; **51** (1983) 534.

[3] NMC collaboration, M. Arneodo *et al.*, Nucl. Phys. **B481** (1996) 23.

[4] K.J. Eskola, Nucl. Phys. **B400** (1993) 240.

[5] T. Gousset and H.J. Pirner, Phys. Lett. **B375** (1996) 349.

[6] A. Mücklich, "The structure function ratio F_2^{Sn}/F_2^C", in Proc. of the Workshop on Deep Inelastic Scattering and QCD, Paris, 1995.

[7] Yu. Dokshitzer, Sov. Phys. JETP **46** (1977) 1649; V.N. Gribov and L. N. Lipatov, Sov. Nucl. Phys. **15** (1972) 438, 675; G. Altarelli, G. Parisi, Nucl. Phys. **B126** (1977) 298.

[8] NMC collaboration, P. Amaudruz *et al.*, Nucl. Phys. **B441** (1995) 3.

[9] NMC collaboration, M. Arneodo *et al.*, Nucl. Phys. **B441** (1995) 12.

[10] NMC collaboration, M. Arneodo *et al.*, Nucl. Phys. **B481** (1996) 3.

[11] J. Gomez *et al.*, Phys. Rev. **D49** (1994) 4348.

[12] E665 collaboration, M.R. Adams *et al.*, Phys. Rev. Lett. **68** (1992) 3266.

[13] E665 collaboration, M.R. Adams *et al.*, Z. Phys. **C67** (1995) 403.

[14] D. M. Alde *et al.*, Phys. Rev. Lett. **64** (1990) 2479.

[15] L.L. Frankfurt, M.I. Strikman and S. Liuti, Phys. Rev. Lett. **65** (1990) 1725.

[16] L.V. Gribov, E.M. Levin and M.G. Ryskin, Nucl. Phys. **B188** (1981) 555; Phys. Rep. **100** (1983) 1; A.H. Mueller and J. Qiu, Nucl. Phys. **B268** (1986) 427.

[17] Jianwei Qiu, Nucl. Phys. **B291** (1987) 746.

[18] H1 Collaboration, I. Abt *et al.*, Nucl. Phys. **B407** (1993) 515; T. Ahmed *et al.*, Nucl. Phys. **B439** (1995) 471; ZEUS Collaboration, M. Derrick *et al.*, Phys. Lett. **B316** (1993) 412; Z. Phys. **C65** (1995) 379.

[19] H1 Collaboration, S. Aid *et al.*, Nucl. Phys. **B470** (1996) 3.

[20] S. Kumano, Phys. Rev. **C50** (1994) 1247. S. Kumano and M.Miyama, Phys. Lett. **B378** (1996) 267; S. Kumano and M. Miyama, Proc. Workshop on Future Physics at HERA, Hamburg, Germany, Sep 1995 and Feb 1996, Preprint SAGA-HE-104-96, [hep-ph/9607246]; M. Miyama, Proc. of Circum-Pan-Pacific Workshop on High-Energy Spin Physics '96, Kobe, Japan, Oct 1996, Preprint SAGA-HE-110-96 [hep-ph/9611221].

[21] D. Indumathi and Wei Zhu, Z. Phys. **C74** (1997) 119; D. Indumathi, Z.Phys. **C76** (1997) 91; D. Indumathi and Wei Zhu, Proc. Workshop on Future Physics at HERA, Hamburg, Sep 1995, preprint DO-TH-96-12, Sep 1995, [hep-ph/9609362].

[22] S. Liuti and R. Vogt Phys. Rev. **C51** (1995) 2244.

[23] Z. Huang, H.J. Lu and I. Sarcevic, Preprint AZPH-TH-97-07, May 1997, [hep-ph/9705250]

[24] A.L. Ayala, M.B. Gay Ducati and E.M. Levin, Nucl. Phys. **B493** (1997) 305.

[25] K.J. Eskola, J. Qiu and X.-N. Wang, Phys. Rev. Lett. **72** (1994) 36.

[26] L. McLerran and R. Venugopalan, Preprint DOE-ER-40561-297, May 1997 [nucl-th/9705055].

[27] P. McGaughey, private communication.

[28] B. Badełek and J. Kwieciński, Phys. Rev. **D50** (1994) 4; Nucl. Phys. **B370** (1992) 278.

[29] S.J. Brodsky and I.A. Schmidt, Phys. Rev. **D43** (1991) 179.

[30] BEBC Collaboration, J. Guy *et al.*, Phys. Lett. **B229** (1989) 421, BEBC WA59 Collaboration, P.P. Allport *et al.*, Phys. Lett. **B232** (1989) 417.

[31] M. Glück, E. Reya and A. Vogt, Z. Phys. **C53** (1992) 53.

[32] G. Smirnov, Proc. ICHEP 96, Warsaw, July 1996 [hep-ph/9611203]; Phys. Lett. **B364** (1995) 87.

[33] C.J. Benesh, J. Qiu and J.P. Vary, Phys. Rev. **C50** (1994) 1015; J. Czyzewski, K.J. Eskola and J. Qiu, in Workshop on Hard Probes of Dense Matter, June 1995, ECT, Trento, Italy.

[34] K. Prytz, Phys. Lett. **B311** (1993) 286.

[35] H1 Collaboration, C. Adloff *et al.*, Nucl. Phys. **B497** (1997) 3.

[36] P. Amaudruz *et al,* Nucl. Phys. **B371** (1992) 553.

[37] M.J. Leitch *et al,* Phys. Rev. Lett. **72** (1994) 2542.

[38] P. Hoyer, M. Vänttinen and U. Sukhatme, Phys. Lett. **B246** (1990) 217; S.J. Brodsky, P. Hoyer, A.H. Mueller and W.-K. Tang, Nucl. Phys. **B369** (1992) 519.

[39] M.A. Braun *at al.*, Nucl. Phys. **B509** (1998) 357.

[40] M. Gonin for the NA50 Collaboration, Proc. *Quark Matter '96*, Nucl. Phys. **A610** (1996) 404c.

[41] CCFR Collaboration, P.Z. Quintas *et al.*, Phys. Rev. Lett. **71** (1993) 1307.

[42] A.D.Martin, R.G. Roberts and W.J. Stirling, Phys. Rev. **D50** (1994) 6734; CTEQ Collab. H.L. Lai *et al.*, Phys. Rev. **D55** (1997) 1280.

[43] P. Hoyer and M. Vänttinen, Z. Phys. **C74** (1997) 113.

[44] R. Kobayashi, S. Kumano and M. Miyama, Phys. Lett. **B354** (1995) 465.

[45] K.J. Eskola and C.A. Salgado, work in progress.

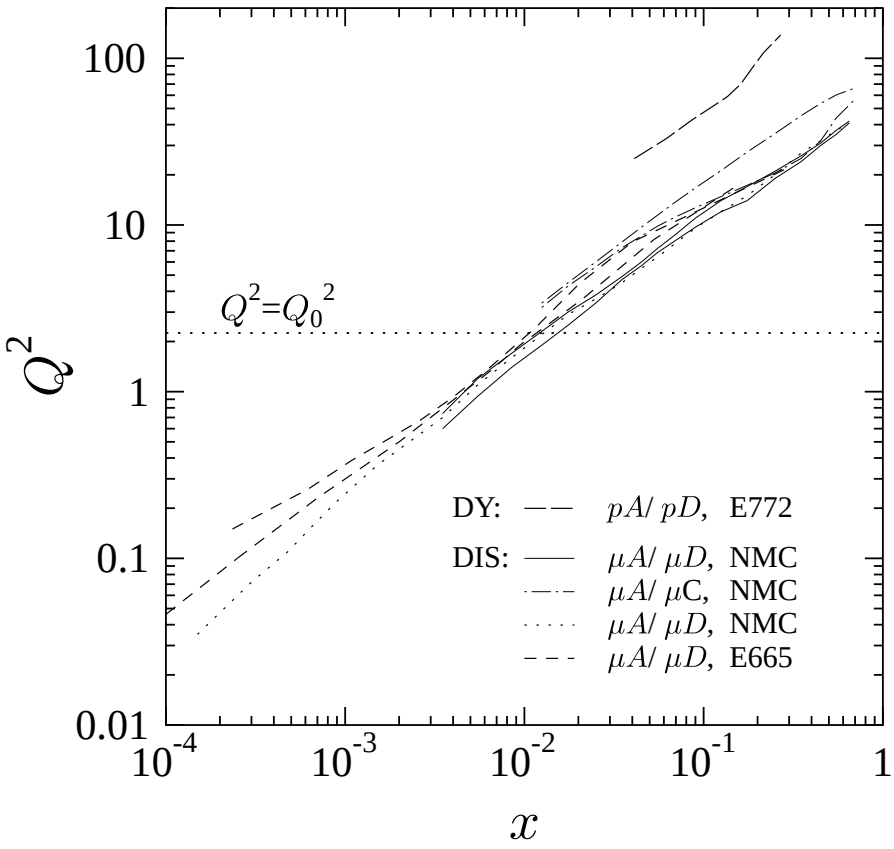

Figure 1: Typical correlation of the scale $\langle Q^2 \rangle$ and x in measurements of $F_2^A(x, Q^2)$ in deeply inelastic lA scatterings and correlation of the invariant mass $\langle Q^2 \rangle$ and $x = x_2$ of Drell-Yan cross sections measured in pA collisions. The correlations in some of the NMC data [8] (solid lines), [10] (dotted-dashed), [9] (dotted) and in some of the E665 data [12] (dashed), and in the E772 data [14, 27] (long dashed) are shown. The horizontal dotted line illustrates the initial scale Q_0^2 we have chosen and above which we perform the DGLAP evolution of nuclear parton densities.

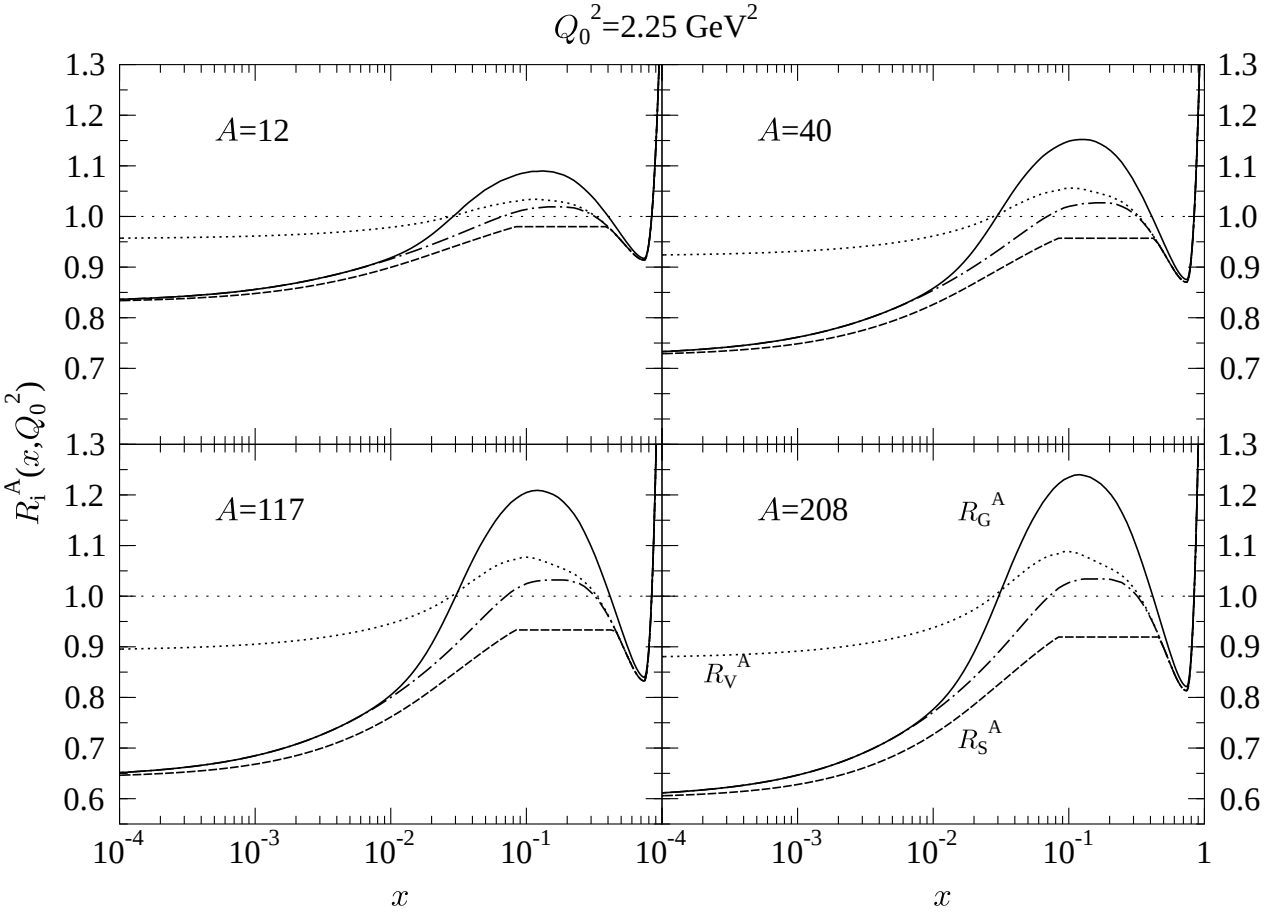

Figure 2: The initial nuclear ratios $R_G^A(x,Q_0^2)$ (solid line), $R_V^A(x,Q_0^2)$ (dotted) and $R_S^A(x,Q_0^2)$ (dashed) for isoscalar nuclei at $Q_0^2 = 2.25$ GeV^2. The ratio $R_{F_2}^A(x,Q_0^2)$ (dotted-dashed) is also shown.

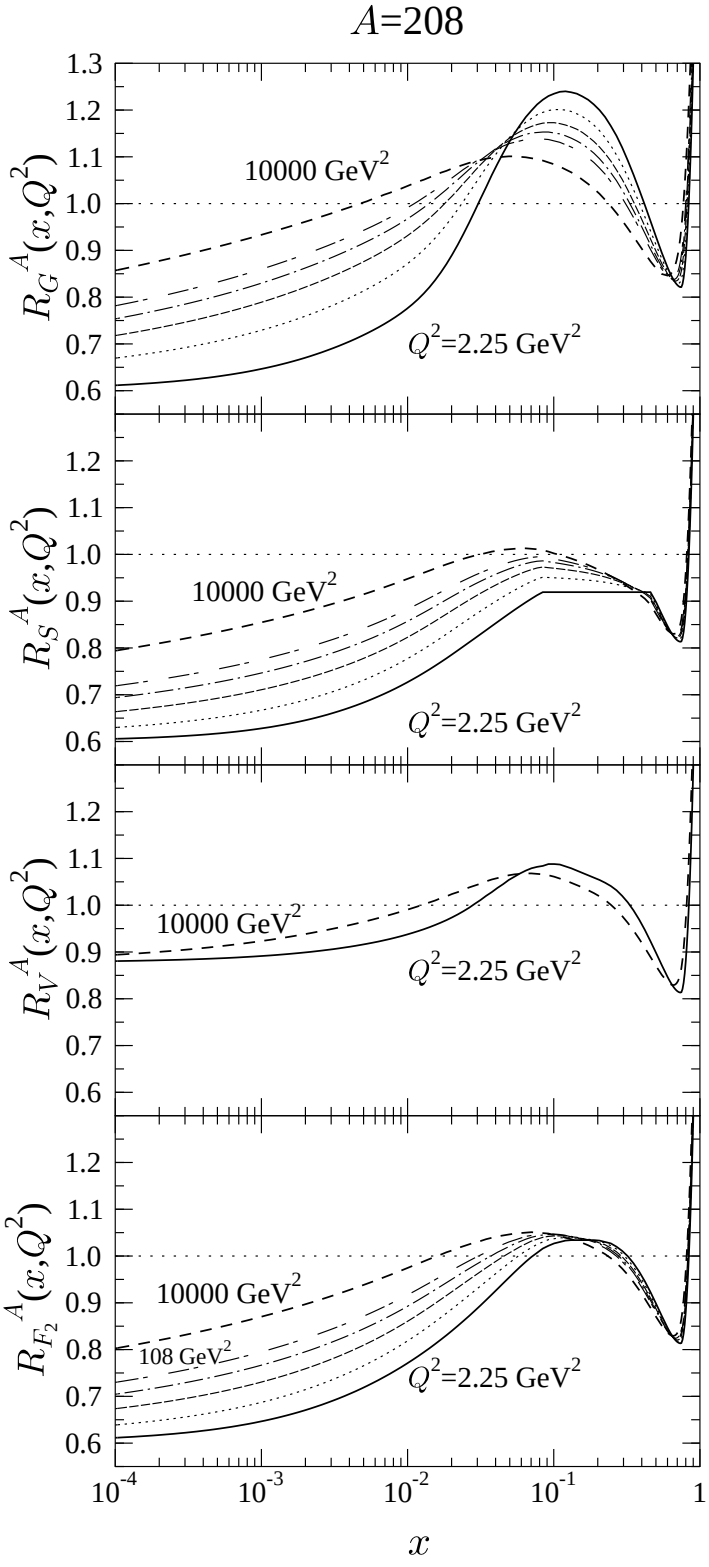

Figure 3: Scale evolution of the ratios $R_G^A(x,Q^2)$, $R_S^A(x,Q^2)$, $R_V^A(x,Q^2)$ and $R_{F_2}^A(x,Q^2)$ for an isoscalar nucleus A=208. The ratios are shown as functions of x at fixed values of $Q^2 = 2.25$ GeV^2 (solid lines), 5.39 GeV^2 (dotted), 14.7 GeV^2 (dashed), 39.9 GeV^2 (dotted-dashed), 108 GeV^2 (double-dashed), equidistant in $\log Q^2$, and 10000 GeV^2 (dashed). For R_V^A only the first and last ones are shown.

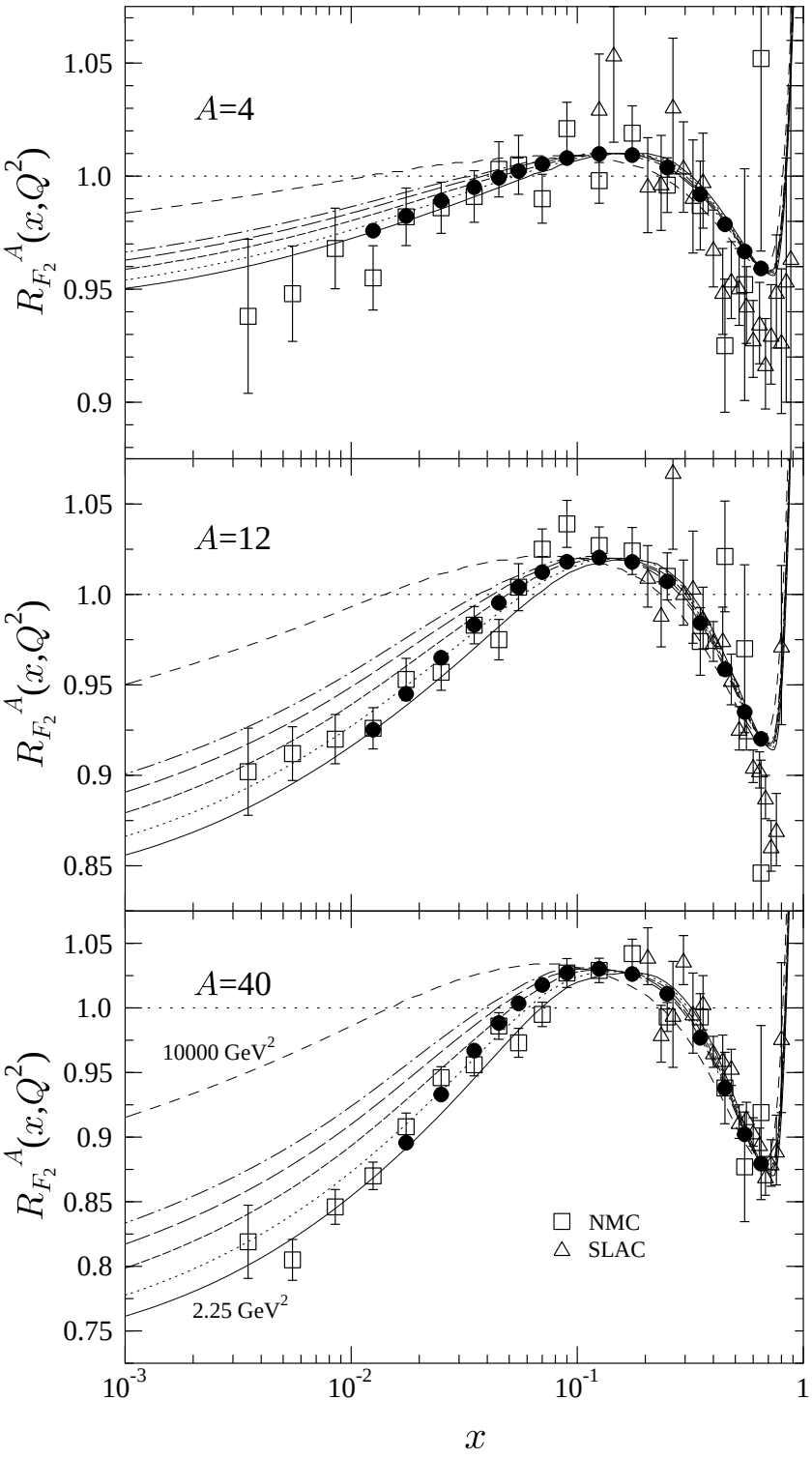

Figure 4: Scale evolution of the ratio $R^A_{F_2}(x, Q^2)$ for isoscalar nuclei A=4, 12 and 40. As in Fig. 3, the ratios are plotted as functions of x but with Q^2 fixed to 2.25, 3.70, 6.93, 12.9, 24.2 GeV^2, equidistant in $\log Q^2$, and 10000 GeV^2. The reanalyzed NMC data [8] is shown by the boxes, the reanalyzed SLAC data by the triangles [11]. The statistical and systematic errors have been added in quadrature. The filled circles show our calculation at the $\langle Q^2 \rangle$ values of the NMC data. Notice that the vertical scale of each panel is different.

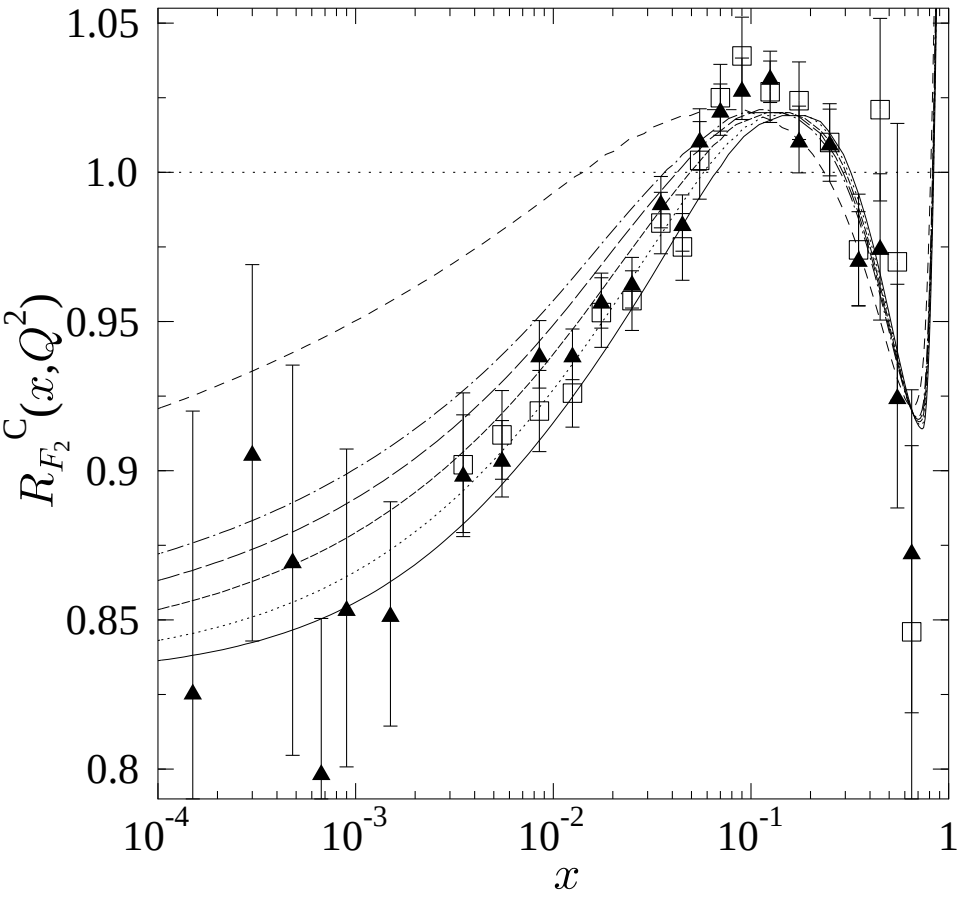

Figure 5: The ratio $R^{\rm C}_{F_2}(x,Q^2)$ shown together with the renanalyzed NMC data [8] (boxes) and the combined NMC data [9] (triangles). The calculated $R^{\rm C}_{F_2}$ are shown at the same fixed values of Q^2 as in Fig. 4. Notice that at $x < 0.01$ the scales $\langle Q^2 \rangle$ of the data are less than our $Q_0^2 = 2.25$ GeV^2. The statistical and systematic errors of the data are added in quadrature.

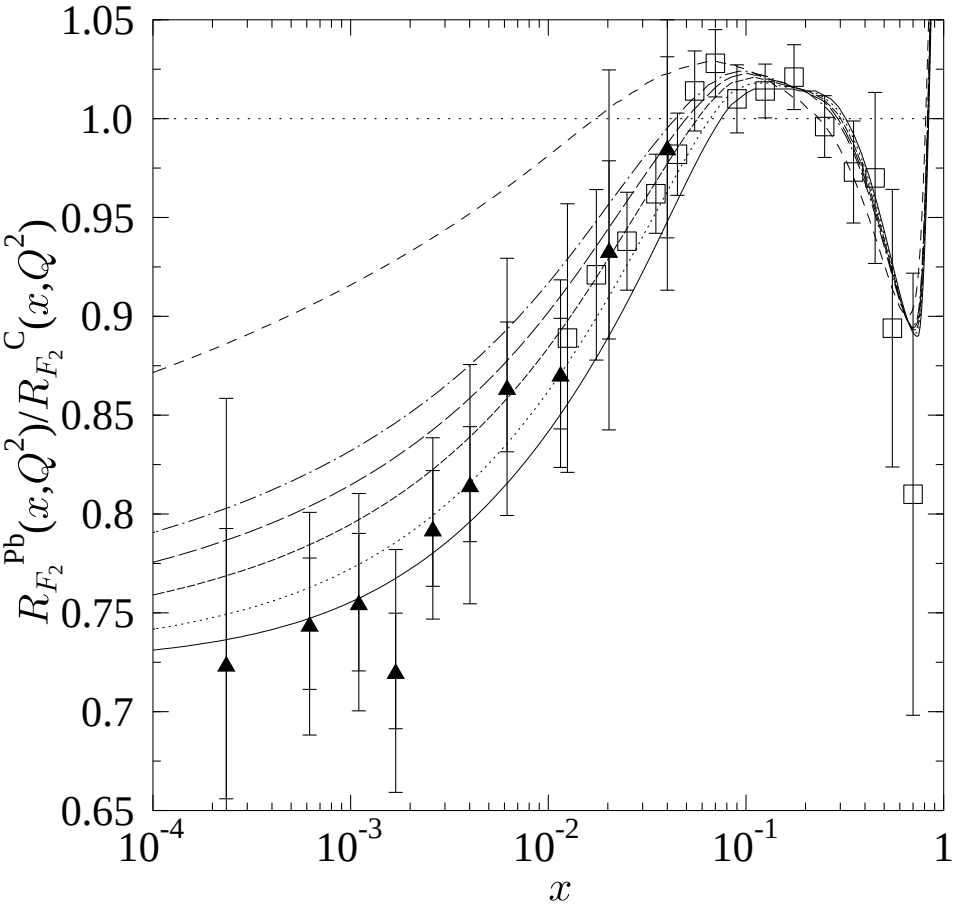

Figure 6: The ratio $R_{F_2}^{\rm Pb}(x,Q^2)/R_{F_2}^{\rm C}(x,Q^2)$ as a function of x at the same fixed values of Q^2 as in Fig. 4. The NMC data for Pb/C [10] is shown by the squares and with statistical and systematic errors added in quadrature. The ratio of the E665 data for $R_{F_2}^{\rm Pb}$ and $R_{F_2}^{\rm C}$ [13] is shown with the triangles. The inner error bars are obtained by including the independent statistical errors only, and the outer ones by adding first the statistical and systematic errors separately for Pb/D and C/D in quadrature, and then taking these errors to be independent. This figure shows how our calculation relates to the small-x region where the measurements are at nonperturbative scales.

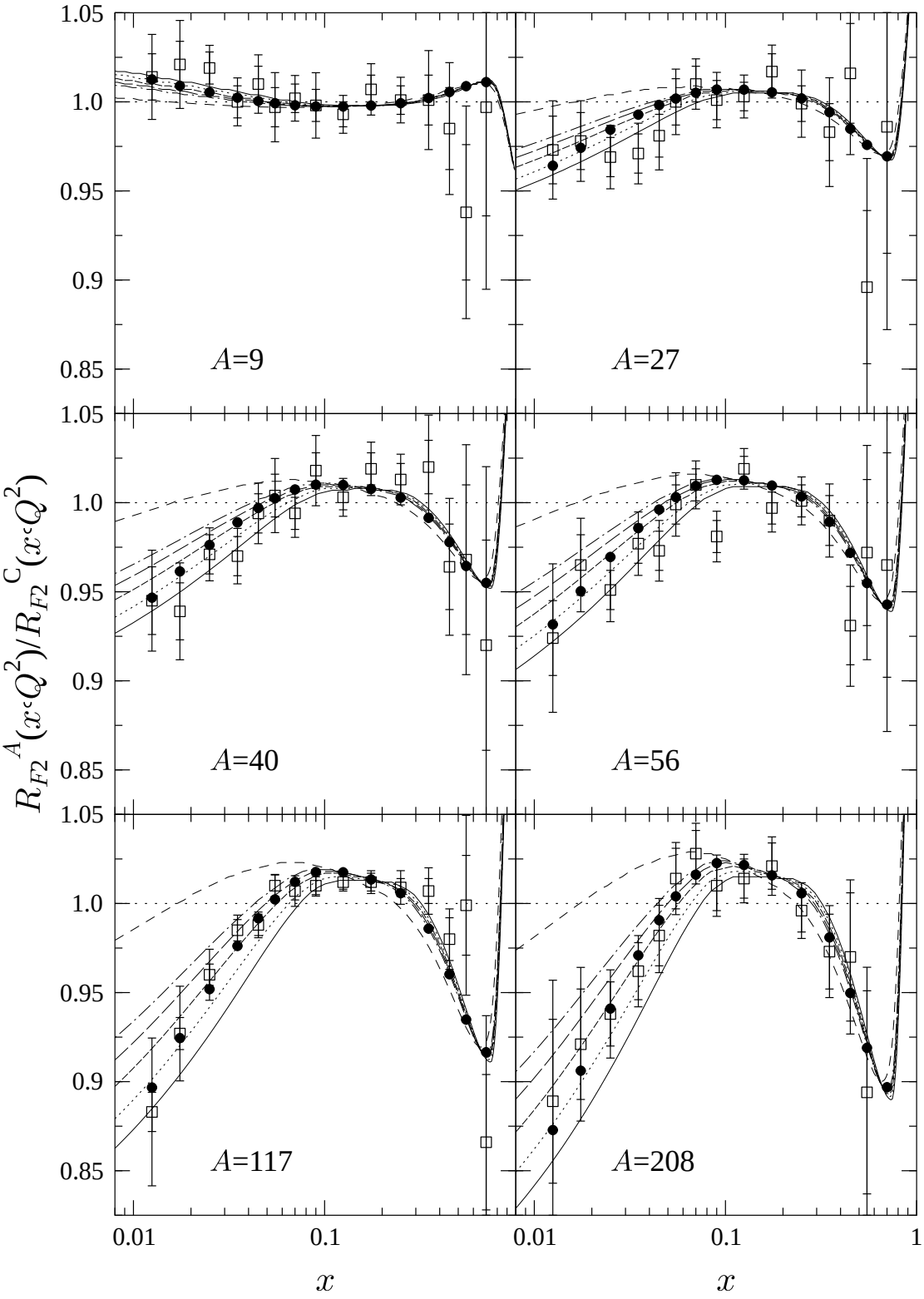

Figure 7: The ratios $R^A_{F_2}(x,Q^2)/R^C_{F_2}(x,Q^2)$ as functions of x for isoscalar nuclei. The values of Q^2 are the same as in Fig. 4. For comparison with the NMC data [10] (boxes), the filled circles show our calculation at the $\langle Q^2\rangle$ of the data. The inner error bars stand for the statistical errors only, the outer ones for statistical and systematic errors added in quadrature.

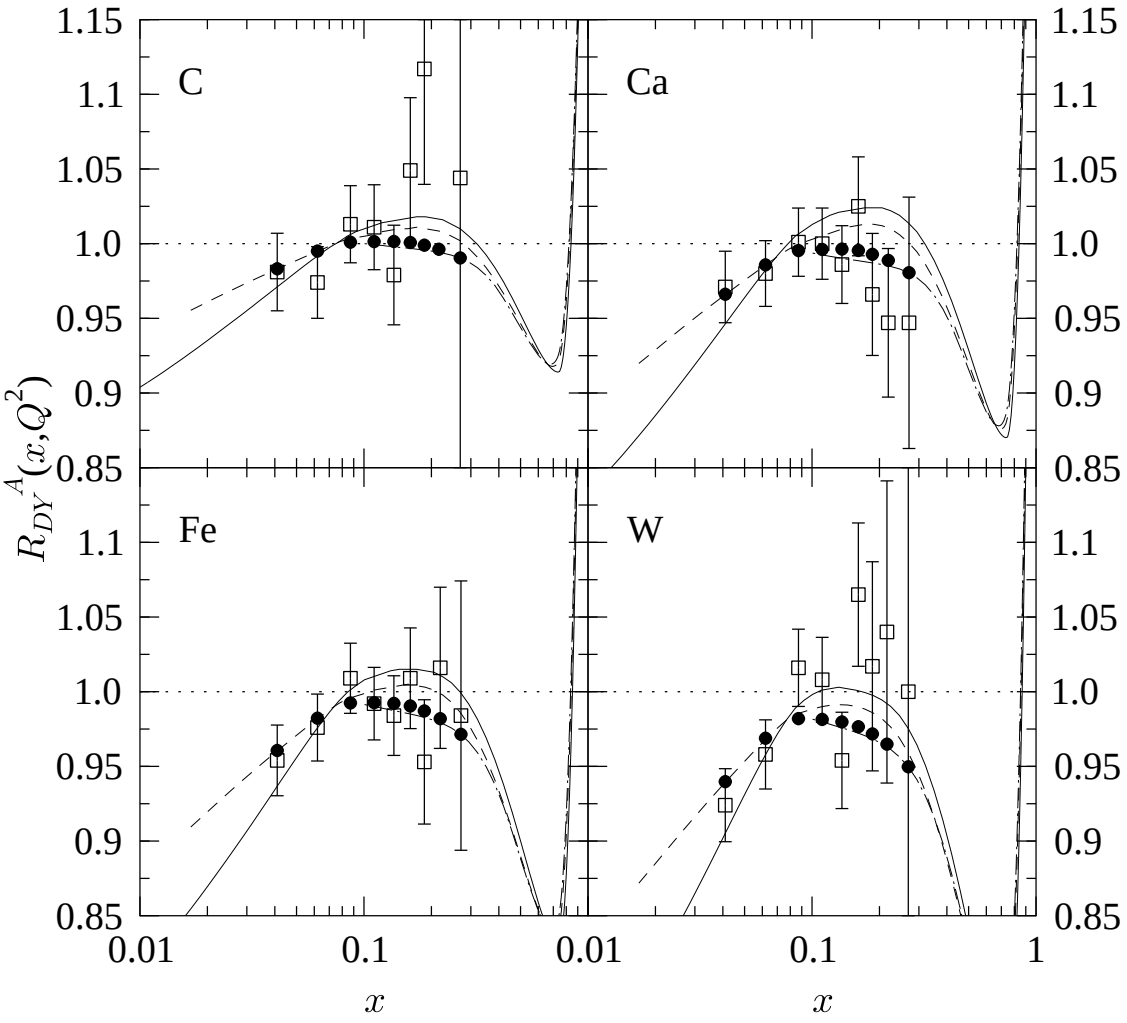

Figure 8: The ratios of differential Drell-Yan cross sections in pA and pD as functions of $x = x_2$ for ${}^{12}_{6}\mathrm{C}/D$, ${}^{40}_{20}\mathrm{Ca}/D$, ${}^{56}_{26}\mathrm{Fe}/D$ and ${}^{184}_{74}\mathrm{W}/D$. Our calculation for $R^A_{DY}(x, Q^2)$ of Eq. (20) is shown at fixed values of the invariant mass $Q^2 = 2.25$ GeV^2 (solid line), 24.2 GeV^2 (dashed), and 139 GeV^2 (dotted-dashed). The data shown by the boxes is from E772 [14]. In the graph the statistical errors and the quoted 2 % systematic errors are added in quadrature. The filled circles show our calculation at the $\langle Q^2 \rangle$ of the data [27].

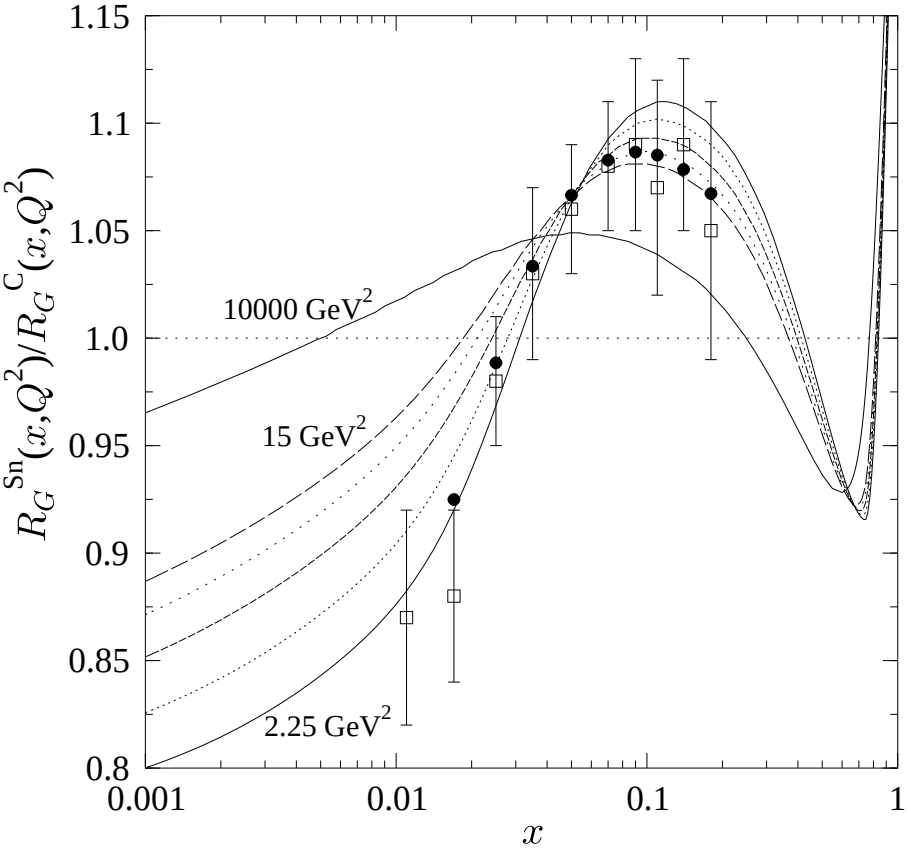

Figure 9: The gluon ratios $R_G^{\rm Sn}(x,Q^2)/R_G^{\rm C}(x,Q^2)$ as functions of x at fixed values of $Q^2 = 2.25$, 3.27, 5.39, 8.89, 14.7 GeV^2, equidistant in $\log Q^2$, and 10000 GeV^2. The filled circles show the comparison with the results of Ref. [5], presented by the boxes.

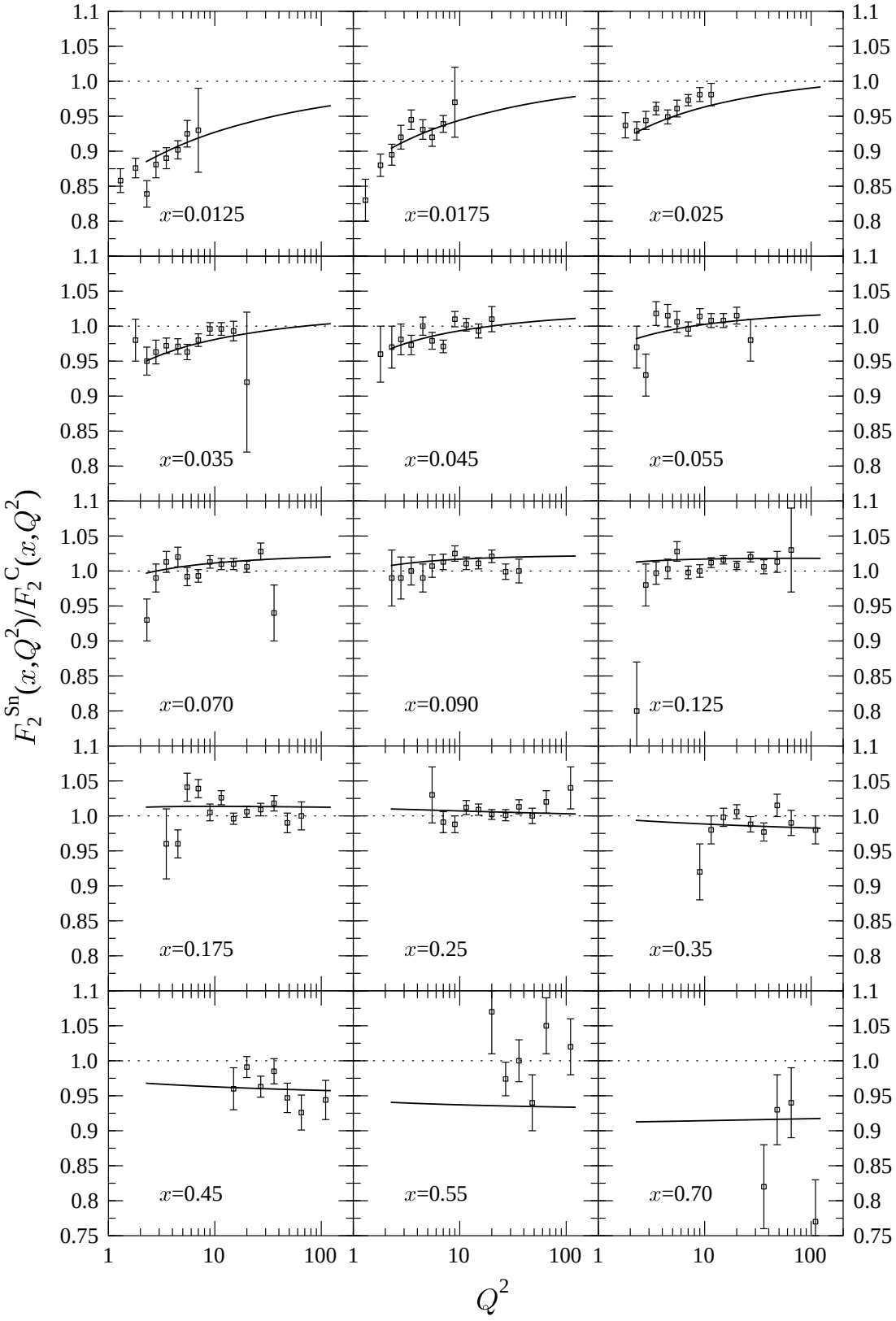

Figure 10: The calculated scale evolution of $F_2^{\rm Sn}(x,Q^2)/F_2^{\rm C}(x,Q^2)$ compared with the NMC data [3] at different fixed values of x. The data are plotted with statistical errors only.